

Inhomogeneous Temperature Fields, Current Distribution, Stability and Heat Transfer in Superconductor 1G Multi-filaments

Harald Reiss¹

Received: 19 December 2015 / Accepted: 20 January 2016 / Published online: 10 February 2016
© Springer Science+Business Media New York 2016

Abstract This paper is focused on simulations of how a superconductor reacts to extreme, suddenly changing operation conditions imposed by strong over-currents. An attempt is made to shed light on the physics of current transport behind, as far as this can be achieved with numerical simulations. For this purpose, temperature and current distribution in multi-filamentary high-temperature superconductors is investigated in a finite element analysis with high spatial and time resolution. An extra subsection is devoted to the involved heat transfer problem. As a result, resistive (Ohmic and flux flow) and zero loss states would co-exist in parallel if over-current cannot be compensated, for example, by switching it to a shunt. Anisotropic thermal diffusivity of high-temperature superconductors, in particular of BSCCO, would obstruct thermalisation of losses, and compensating of field and current in-homogeneities would become impossible within acceptable periods of time.

Keywords Superconductor · Finite element analysis · Local conductor temperature · Random variables · Current distribution · Conductor stability · Heat transfer · Current percolation

1 Survey

When investigating current propagation in superconductors, a standard assumption is to consider temperature and current

distribution in conductor cross sections as homogeneous, compare traditional volumes on theory of superconductivity like [1–3] or more recent contributions on applied superconductivity, for example [4–6]. While all these volumes consider *temperature dependence* of superconductor materials properties, they at the same time assume homogeneity of temperature and current *distribution*. The number of theoretical and experimental reports that apply the same simplifying assumption is almost unlimited. The question is whether this is fulfilled, in reality, in low- and high-temperature superconductors and in any conductor geometry.

A numerical (finite element) analysis of temperature fields, current distribution and stability against quench recently was presented in [7] for a 1G high-temperature superconductor. Results demonstrated that, under large current load, conductor temperature and transport current distribution may become highly inhomogeneous, with temperature variations in the conductor cross sections in the order of dozens of Kelvin and with corresponding impacts on conductor stability. While [8] investigated a thin film (monolithic) conductor, the present paper addresses *multi-filamentary* geometry and takes in account also the strong anisotropic materials properties of the high-temperature superconductor BSCCO (2223).

In a first numerical approximation, the finite element (FE) analysis presented in [7] was limited to a quasi-*continuum*, cylindrical conductor model. As a second compromise, the analysis had to apply a *model* conductor suitable for manufacture of 1G filaments but with essentially the materials properties of YBaCuO. Thermal diffusivity, electrical resistance and critical current density of BSCCO, though highly desirable, were not available over the wide range of temperature necessary to cover the whole field between zero resistance and flux flow and Ohmic resistive

✉ Harald Reiss
harald.reiss@physik.uni-wuerzburg.de

¹ Department of Physics, University of Wuerzburg,
Am Hubland, 97074 Wuerzburg, Germany

states. Meanwhile, both problems have partly been overcome, and the present paper introduces FE simulations with strongly improved spatial resolution and applies proper, anisotropic materials properties of BSCCO (2223).

Figure 1a shows cross section of the “first generation” (1G) BSCCO Long Island conductor [9], the operation of which in the following shall be simulated under nominal and, as a disturbance, under large over-current. Figure 1b presents the corresponding FE scheme (the figure shows only the left half of the total, multi-filamentary conductor cross section).

The simulations are applied to a bundle of identical multi-filamentary conductors all switched in parallel. Like in [7], the bundle is integrated into an electrical circuit that allows comparison with a similar system described in [10] with same root mean square phase voltage and same conductor cross section. We could instead take *any* large- or small-scale electrical grid, like in a laboratory experiment, with an appropriately dimensioned superconducting component; the point is the physics of transport processes behind. The paper is focused on simulation of extreme operation conditions; an extra subsection had to be devoted, under these conditions, to the involved, transient heat transfer problem.

2 Description of the Numerical Calculation Steps

The numerical concept is as before (mapped meshing, same thermal boundary conditions and FE solution scheme); it is applied to a single 1G conductor, with the exception that we in the present paper provisionally neglect dependency

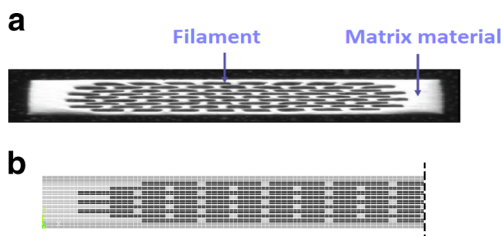


Fig. 1 a, b Cross section (a, above) of the 1G BSCCO 2223/Ag Long Island Cable superconductor [9] and finite element model (b, below) of the left half of the conductor cross section showing superconductor filaments (black) and matrix material (Ag, light grey). The thick, dashed dotted line denotes axis of symmetry. A number $N = 91$ identical filaments is integrated in the total cross section of one multi-filamentary conductor, and a number $M = 196$ of identical conductors (switched in parallel) is bundled to a cable, with 10^{-4} m² total superconductor cross section. Thin white lines indicate finite element mesh ($N_{El} = 4032$ in this case, compare text). Dimensions of filaments and of conductor in x (horizontal) and y (vertical) directions are $x = 280 \mu\text{m}$ (filament) and 3.84 mm (total conductor width) and $y = 20 \mu\text{m}$ (filament) and $264 \mu\text{m}$ (total conductor thickness), respectively

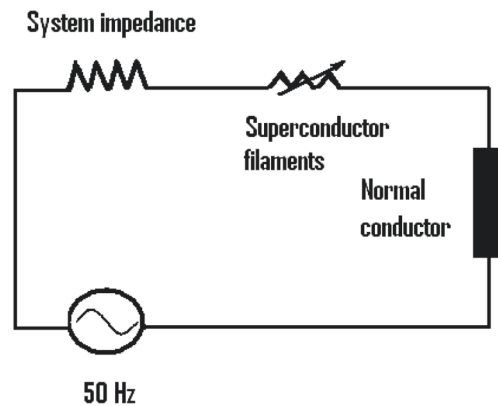


Fig. 2 Schematic view of an electrical grid for numerically testing how a superconductor multi-filamentary wire reacts to a sudden current load increase. The circuit in this figure either refers to a small-scale laboratory experiment, or in large scale, to a medium voltage distribution system. The normal conductor of resistance R_{NC} serves as an auxiliary variable; it is assumed its sudden decrease, within 2.5 ms to finally 1/20 of its original magnitude, initiates increase of transport current to a multiple of its nominal value (a fault). In the present calculations, voltage, conductor cross sections and impedance are the same as in [10]. The figure is taken from [7]

of materials parameters on z -positions (Fig. 1b; the conductor and its performance shall be homogeneous over its total length); otherwise, computation time would increase too strongly. It is assumed the conductor is located near the periphery (close to the coolant) of a bundle of 196 identical conductors. Each conductor incorporates 91 BSCCO filaments (black rectangles in Fig. 1b). The matrix material again is Ag. With the dimensions indicated in the caption to Fig. 1b, the ratio of superconductor to total 1G conductor cross section amounts to about 0.45.

2.1 Data Input

Electrical resistances of the superconductor filaments cover Ohmic, inductive, flux flow, hysteresis and, within the Ag matrix material, coupling resistances. All parameters of the conductor applied in the simulations take into account cross-wise physical dependencies, like T_{crit} vs. $B_{\text{crit}1,2}$ or $B_{\text{crit}1,2}$ vs. T , or thermal diffusivity vs. temperature, T .

Modelling of Ohmic resistive states is straight-forward. The specific Ohmic resistance of BSCCO 2223 material is shown in Fig. 10 in the Appendix. Critical temperature, T_{crit} , of solid BSCCO (2223) is 108 K (mean value), at very small magnetic field. Modelling of flux flow resistivity to axial current is again made according to [11, 12]. Weak link, grain boundary structure of a polycrystalline conductor constitutes potential obstacles to current flow in z -direction that is laid upon its solid constituents. But the obstacles not only concern electrical transport (electron charges). Also magnetic (movement of vortices, well known as flux flow)

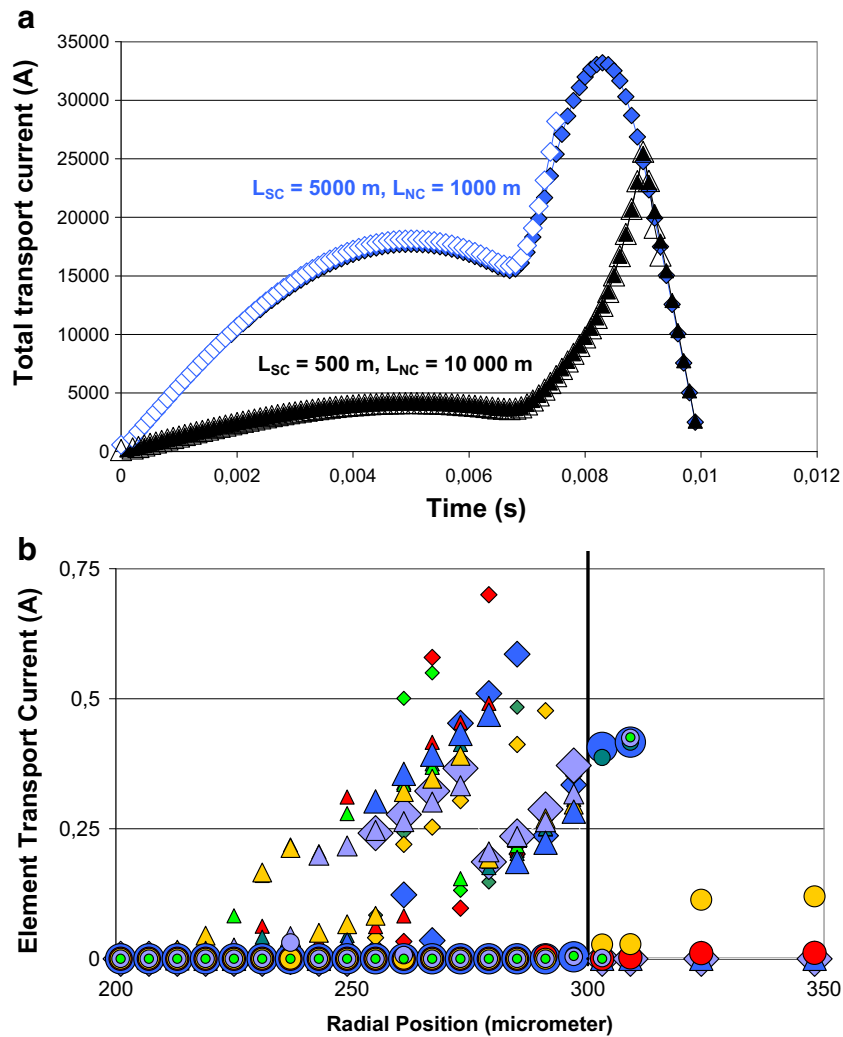


Fig. 3 **a** Comparison of the results for total transport current obtained in [7], Fig. 8 (solid blue diamonds and solid black triangles), and in the present paper (open symbols). Results are given for different conductor lengths, L_{SC} , and different normal resistances $R_{NC} = 0.18$ and 1.8Ω indicated by the lengths L_{NC} of 10^3 and 10^4 m, respectively, and using the specific resistance $\rho_{Cu} = 1.8 \cdot 10^{-8} \Omega \text{ m}$ of Cu and a cross section, $A_{NC} = 10^{-4} \text{ m}^2$ (compare the circuit in Fig. 2). As explained in the text, the results from [7] were calculated using a cylindrical geometry and a model conductor while the data obtained in the present paper result from the conductor geometry shown in Fig. 1b but with same (model) materials properties. Accordingly, the comparison, to be made separately in blue and black symbols, is between two different finite

element models, not between different conductor materials. **b** Distribution of transport current (nominal plus fault) in planes $z = \text{const}$ in the cylindrical filament modelled in [7]. Solid diamonds, triangles and circles correspond to $t = 3, 6$ and 9 ms, respectively, after start of the simulations. Results are plotted in dependence of radial position (the vertical black line at $300 \mu \text{m}$ separates superconductor, left part of the figure, from matrix material). Axial positions (z -direction in Fig. 1b) of the planes are identified by different colours: blue, red, dark green, light green, dark yellow and lilac symbols correspond to $0.1, 0.7, 1.3, 1.9, 2.5$ and 3.1 mm distance from the lower end of the conductor, respectively

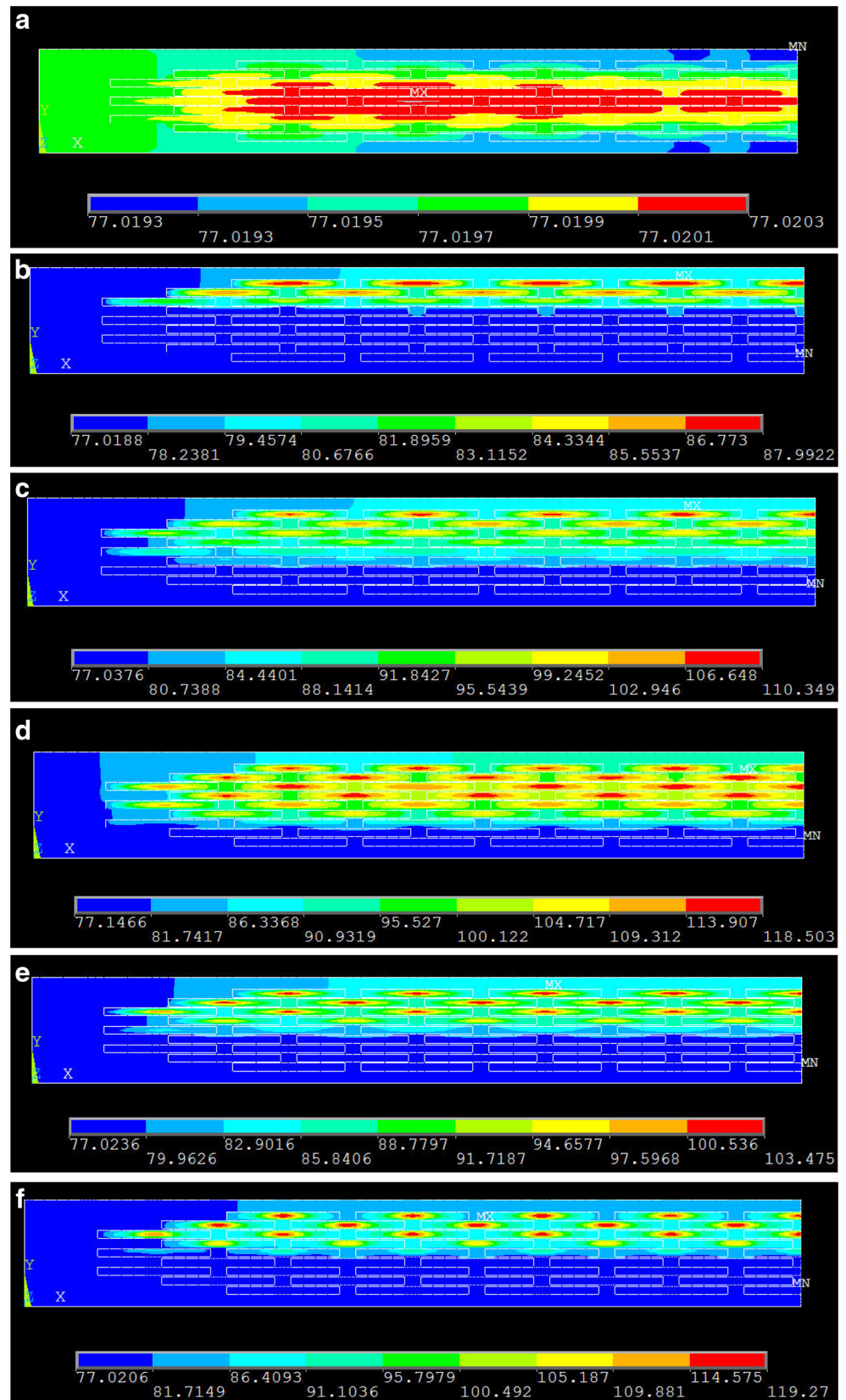
and thermal transport is subject to obstacles induced by a grain boundary structure.

Resistance to magnetic transport has to be considered separately in grains and in grain boundaries. A schematic, rather optimistic, c -axis orientation of plate-like grains that constitute the filaments, and a circumferential magnetic field, under axial (z -) direction of current, is assumed. Flux

flow, under this condition, would occur in horizontal (x -) directions only.

The low-temperature, empirical relation, $\rho_{FF} = \rho_{NC} B/B_{\text{crit},2}$, between specific resistivity of flux flow, ρ_{FF} , and normal conduction, ρ_{NC} , should be applicable to also high-temperature superconductors, as explained in [11]. However, this relation is valid for superconductor solids,

Fig. 4 **a–d** Temperature field (nodal temperatures) in the cross section of the BSCCO (2223) multi-filamentary conductor observed at the beginning ($t = 6.5$ ms, *top*) and at $t = 7.9$, 8.5 and 8.6 ms (*below*), with 1.4, 2.0 and 2.1 ms after start of the disturbance, respectively. Temperatures are identified by the corresponding *horizontal bars*. Symbols *MX* and *MN* indicate positions in the cross section where minimum and maximum temperature is observed. The number of elements is $N_{El} = 4032$. **e, f** Temperature field calculated with $N_{El} = 1440$ (*above*) and 12384 (*below*) elements; data are plotted at 1.7 ms after start of the disturbance. The figure serves for comparison of results when the number of elements, N_{El} , is strongly different



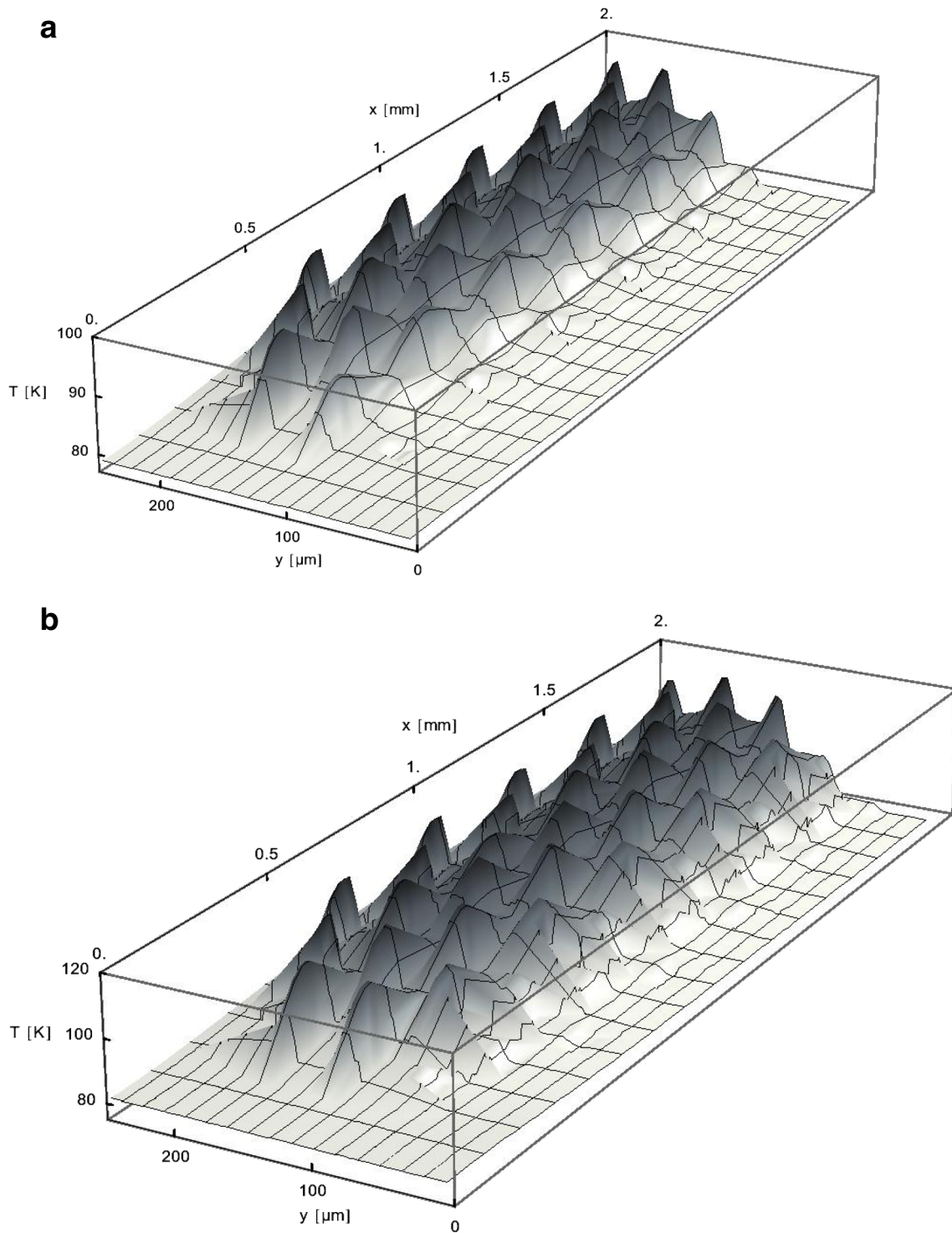


Fig. 5 **a, b** 3D-plot of temperature field in the cross section of the BSCCO (2223) multi-filamentary conductor observed at $t = 8.3$ (*top*) and 8.6 ms (*below*), 1.8 and 2.1 ms after start of the disturbance, respectively. The number of elements is $N_{El} = 4032$

not to a network of solid particles surrounded by weak link, possibly porous materials shells. The overall structure of this relation shall be maintained but modifi-

cations like in [7] are applied to this expression to account for weak-link behaviour. Details of the method will be reported elsewhere. The result, axial resistivity,

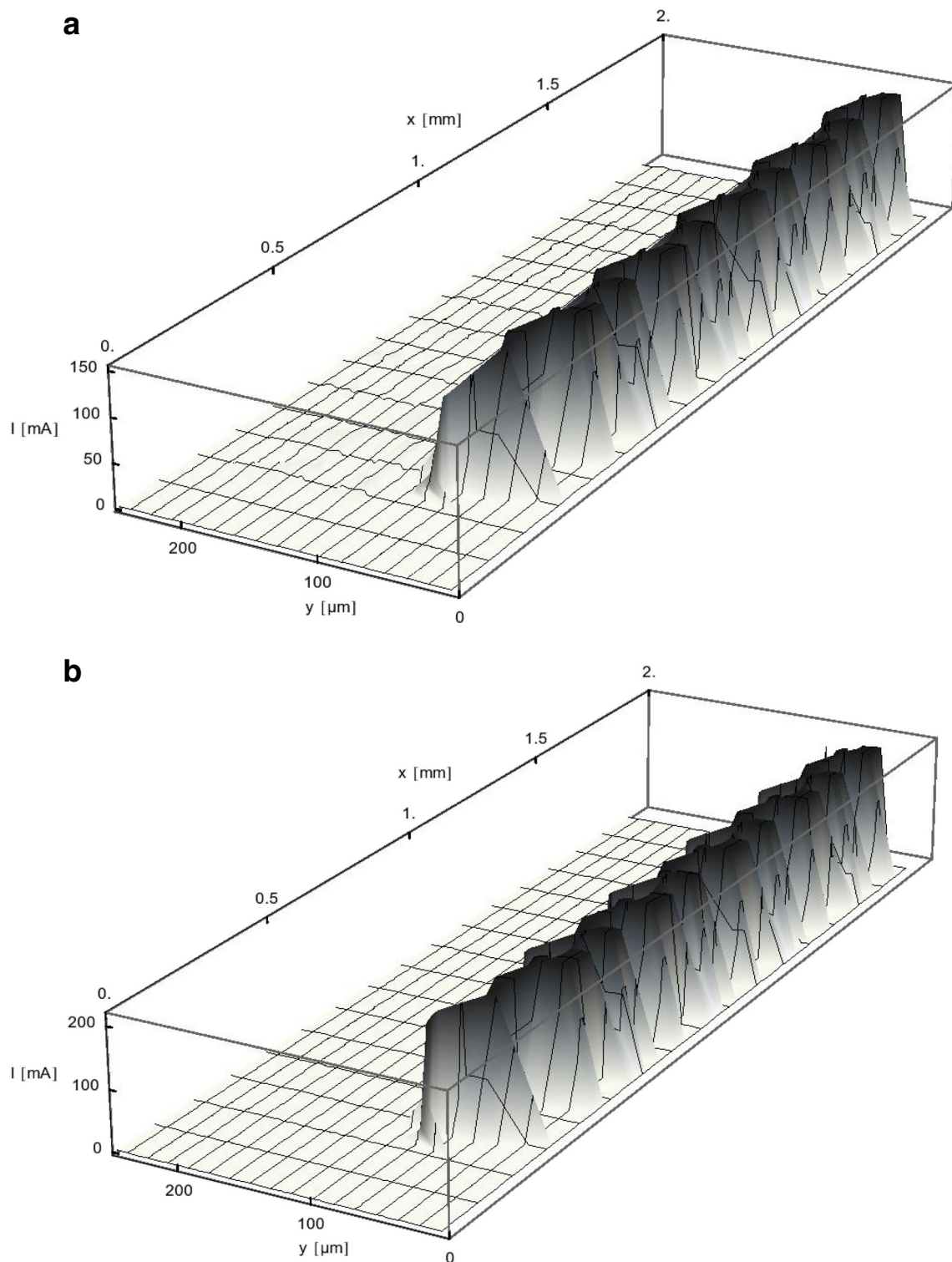


Fig. 6 **a, b** 3D-plot of transport current in the cross section of the BSCCO (2223) multi-filamentary conductor observed at $t = 8.3$ (*top*) and 8.6 ms (*below*), 1.8 and 2.1 ms after start of the disturbance,

respectively. The number of elements is $N_{EI} = 4032$. Comparison with Fig. 5a, b confirms that transport current, as is to be expected, avoids flowing through elements of high temperature

ρ_{FF} , to current transport, under horizontal flux flow in the porous, poly-crystalline, roughly layered, material, is

shown in Fig. 11 (see [Appendix](#)). The resistivity ρ_{FF} is larger than ρ_{NC} , contrary to what would be expected from

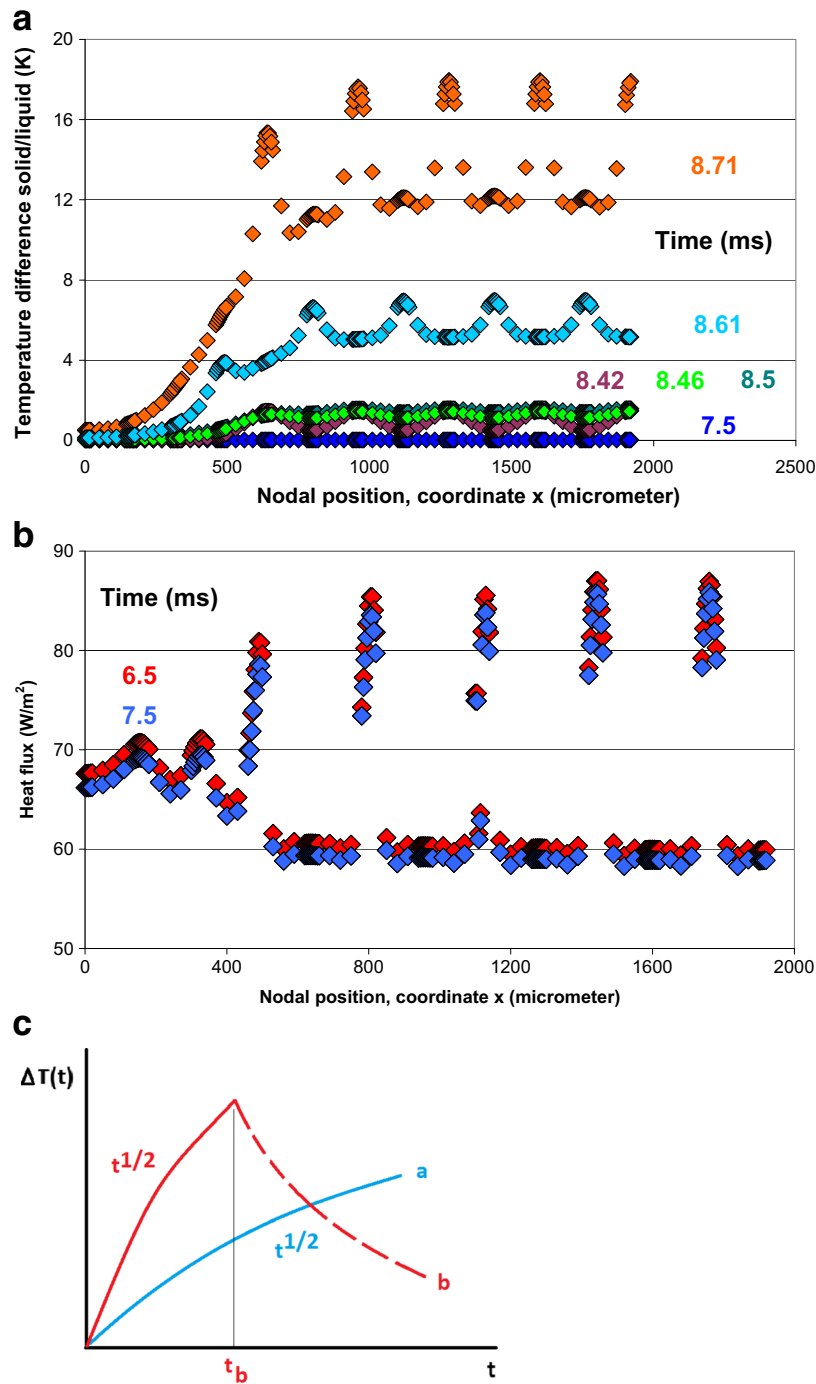


Fig. 7 **a** Temperature difference (nodal values), ΔT , at the solid/liquid interface, at increasing time, vs. nodal position (x -coordinate) on the conductor surface. Location of the ΔT reflects position of the filaments (hot spots) in the conductor. Increase of the ΔT is due to increasing thermal load. Note that location of the temperature maxima depends on time. The thick Ag-“block”, with smaller volume density of heat sources in the interior of the conductor, is on the left (compare Fig. 1b). The number of elements is $N_{EI} = 12384$. **b** Heat flux, dq/dt , emitted in y -direction from Ag-surface elements to the coolant, at increasing time, vs. nodal position (x -coordinate) on the conductor surface. Like in **a**, location of peak heat flux values reflects position of the filaments in the conductor. Data are given at $t = 6.5$ (start of the disturbance) and 7.5 ms (red and

blue diamonds, respectively). In both cases, heat transfer is by convection only, while at $t > 8$ ms, the calculated heat flux would increase too strongly (beyond 10^6 W/m²) to allow application of the stationary heat transfer data from [15], and any adiabatic assumption would be erroneous. The number of elements is $N_{EI} = 12384$. **c** Dependence of temperature difference, ΔT (schematic), at the heated solid/coolant interface, on time and on thermal load (cases *a* and *b*, given as parameter). Load (*b*) exceeds load (*a*), both of constant strength (W/m²). Deviation of curve (*b*) from the $\Delta T \sim t^{1/2}$ -relation at the time t_b indicates onset of boiling (strictly speaking: onset of heat transfer mechanisms other than conduction or convection as long as these would follow a linear $dq/dt \sim \Delta T$ -law, at all times)

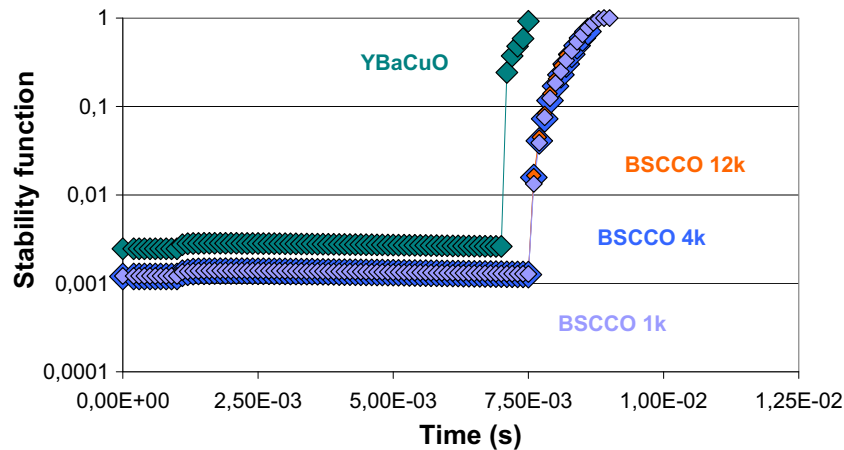


Fig. 8 Stability functions calculated for a BSCCO (2223) multifilamentary conductor (and, for comparison, using YBaCuO materials properties). Both calculations were performed in the same 1G conductor geometry (same finite element scheme; manufacture of a 1G conductor using YBaCuO is impractical, however, and the results obtained for YBaCuO simply reflect the lower T_{crit}). All results (BSCCO) are calculated with identical conductor length, $L_{\text{SC}} = 5000$ m, and with a

normal resistance, $R_{\text{NC}} = 1.8 \Omega$ (compare the circuit in Fig. 2) using the specific resistance $\rho_{\text{Cu}} = 1.8 \cdot 10^{-8} \Omega \text{ m}$ of Cu, a cross section, $A_{\text{NC}} = 10^{-4} \text{ m}^2$, and length $L_{\text{NC}} = 10^4$ m. Results indicated with BSCCO 1, 4 and 12 k have been obtained with increasing number of elements, $N_{\text{El}} = 1440, 4032$ and 12384 (lilac, dark blue and light red diamonds, respectively). For YBaCuO, $L_{\text{NC}} = 10^3$ m, $N_{\text{El}} = 4032$

the standard assumption, but it accounts for transport of current *under flux flow conditions* in a series of obstacles constituted by both solids *and* weak links. The comparatively large ρ_{FF} not necessarily indicates strong flux pinning.

Thermal diffusivity, D_{Th} , of the BSCCO solid superconductor material is between about $1.2 \cdot 10^{-5}$ and $5.9 \cdot 10^{-6} \text{ m}^2/\text{s}$ in the ab-conductor plane, at temperatures of 77 and 120 K. Thermal conductivity and specific heat are given in Figs. 12 and 13, respectively; see Appendix. This is much smaller than the magnetic/electrical diffusivity, $D_{\text{El}} = \rho_{\text{NC}}/\mu_0 \approx 10 \text{ m}^2/\text{s}$, of solid superconductor material under normal (Ohmic) conduction. If, for example, $T = 110$ K, the characteristic times, τ , at this temperature are $\tau_{\text{El}} = 3.9 \cdot 10^{-12}$ and $\tau_{\text{Th}} = 5.5 \cdot 10^{-6}$ s, respectively, in the grains. Current redistribution thus occurs quasi-instantaneously, while diffusive thermalisation of losses from disturbances that propagate through the poly-crystalline network takes much longer. This inevitably leads to at least transient inhomogeneous conductor temperature distributions, except perhaps in elements located closely to the solid/liquid interface to the coolant or to another heat sink provided coupling to the heat sinks is strong. The question is how long it would take a conductor, with anisotropic thermal transport properties, to smooth out such temperature variations under continuous high load (this is not simply a straight-ahead cool-down of a conductor with initially increased, but homogeneous temperature distribution).

Like in our previous reports [7, 13, 14], we use data for heat transfer from metallic surfaces to boiling LN₂

[15] including its dependency on temperature and circumferential position. If there were isolated, oscillating single heat sources within the filament volumes, oscillations of $T(x, y, t)$ at the solid/liquid interface again would be small. But heat sources in the present case are *distributed* in the conductor (see Fig. 4a–f), and as soon as there is current sharing from superconductor to matrix material, heat sources will be located not only in the interior of the conductor but in close neighbourhood of the solid/liquid interface, at distances only a few micrometres away.

The same heat transfer data were applied in [8] to ceramic superconductor and polymer surfaces. Though the obtained successful overall comparison with experiment is remarkable, this assumption yet might be questionable. Original data [15], Fig. 104, were obtained on optically smooth, metallic surfaces and under stationary (not periodic) boundary conditions.

2.2 Calculation Scheme

We will again apply *random* critical superconductor parameters (critical temperature, current density, magnetic field, weak link behaviour), as a method to account for shortages in materials development, manufacture and handling of the sensitive 1G conductors (for example, micro-pores and cracks might come up during winding). The Meissner effect will be checked separately in each of the finite elements (several thousands) of the numerical calculation scheme.

As previously, a divisor, $N_{\text{Cut off}}$, applied to total AC resistance of the electrical circuit, beginning at $t = 6.5$ ms after start of the simulation with $N_{\text{Cut off}} = 1$, gradually

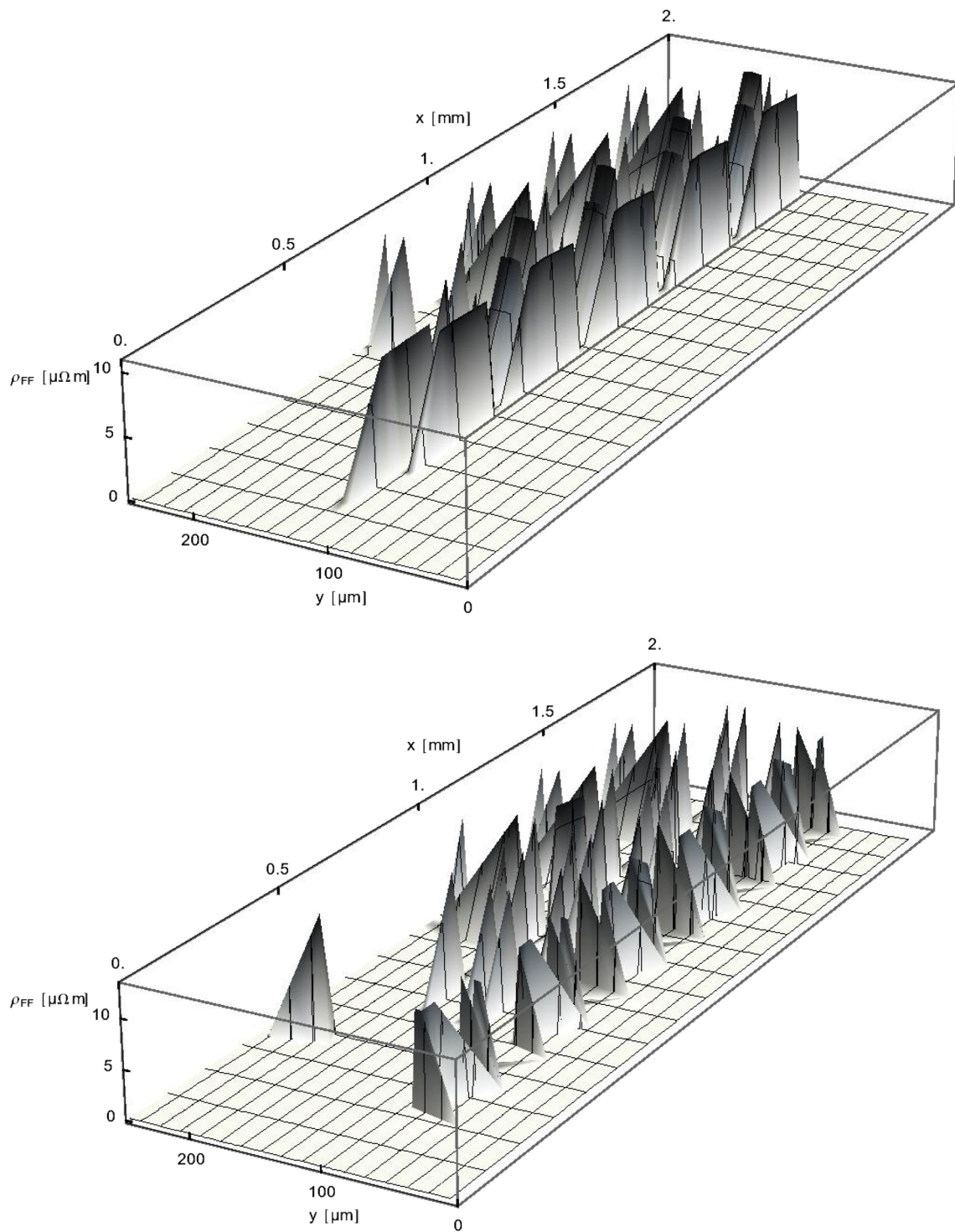


Fig. 9 Distribution of specific flux flow resistances, ρ_{FF} , in the BSCCO (2223) conductor cross section; results are observed at $t = 8.3$ and 8.6 ms (1.8 and 2.1 ms after start of the disturbance), respectively. The number of elements is $N_{El} = 4032$

increases from its initial value to the final $N_{Cut\ off} = 20$, at $t = 9$ ms, and then is kept constant. The variation of $N_{Cut\ off}$ accordingly simulates a fault.

The present calculations can be considered a starting point for simulation of current propagation in general. We wish to demonstrate the existence of strongly

in-homogeneous temperature fields in an 1G multi-filamentary superconductor and the consequences for current transport. Design calculations of current limiters or of other technical devices are not the aim of this paper.

2.3 Solution Scheme

The solution scheme applies the finite element programme Ansys 16. The FE programme is embedded into an overall, four-level calculation scheme explained in [7], Section 2.2.

Accuracy of the FE method to a large extent belongs on adequate meshing. The total number N_{EI} of elements in the half cross section (Fig. 1b) was between 1440 and 12384. Though the $N_{\text{EI}} = 1440$ mesh yields overall agreement with integral results like total transport current, distribution of hot spots, stability functions that were obtained with larger N_{EI} , its resolution was too coarse for a detailed study of temperature and current distributions. The number $N_{\text{EI}} = 4032$ probably is the smallest that can be tolerated for transient simulations in this complicated conductor geometry (and this, too, is an economical measure).

Temperature fields that result from three different N_{EI} are shown below (compare Figs. 4d vs. e, f). Overall agreement is seen concerning position of hot spots, but the larger the number N_{EI} (the finer the spatial resolution), the more will peak temperature dominate over temperature of neighbouring elements. Yet almost no differences between the three N_{EI} are observed in the calculated stability functions (Fig. 8).

Computation time became increasingly impractical on a standard PC (4-core processor) when using $N_{\text{EI}} > 10^4$. Total simulated period then had to be limited to about $t \leq 12.5$ ms. It took about 26 h to simulate this period (this is in the same order or magnitude as reported in [8] for investigation of a thin film superconductor with less complicated geometry).

The total period (one swing of 20 ms) has been split into 200 equal length periods, $\Delta t = 10^{-4}$ s. To obtain convergence, the procedure within each Δt had to be split into up to $N = 10$ sub-steps of appropriate, variable length. Integration time δt within each sub-step $\Delta t/N \geq 10^{-5}$ s is between 10^{-14} and 10^{-7} s; convergence shall be achieved at the end of each sub-step and, finally, at the end of each ΔT period. This procedure reflects the strong non-linearity of almost all involved parameters and transport processes. It yields a series of converged, quasi-stationary solutions.

Within the period $t \leq 12.5$ ms (up to 6 ms after start of the disturbance), no divergences ($T < 77$ K, or run-away to extremely high temperature) were observed that could result from too large $\Delta t/N$ and δt , or from a mismatch between δt and size of element volumes. After repeated (re-)distributions of total transport current to the finite elements

(each of them considered, in a geometrical sense, a current carrying “channel” in z -direction), transport current density taken within each element finally converges to critical current density, the standard requirement to be fulfilled with operation of superconductors, with any over-current switched to the Ag-matrix.

In-homogeneity of temperature and thus of current distribution becomes obvious already for times $t = 2$ or 3 ms after start of the disturbance; see below, Section 3. If over-current is not eliminated, for example, by shifting it to a shunt, hot spots cannot be compensated by only thermal capacity of conductor and matrix material or by heat transfer to the coolant. The questions then are, from the solely *physics* aspects, which type of resistances really is obtained in the volume, whether a shunt or equivalent experimental measures inevitably would be necessary, and which type of resistance then could be responsible for switching an over-current to the shunt. In particular, it is not clear whether current limitation by solely flux flow resistance could successfully be realised at all.

2.4 Conductor Geometry, Critical and Depairing Current Density

Total conductor length is 5000 m; this assumption from [7] tends to current limitation by flux flow resistance. A mean value of $J_{\text{Crit}} = 3.75 \cdot 10^8$ A/m² at $T = 77$ K and at magnetic field $B = 100$ mT is applied again (this is referenced to as the “higher” J_{Crit} in [7]). Depairing current density, J_{D} , is shown in Fig. 14 in the Appendix. At temperature close to critical temperature, we have the Ginzburg/Landau relation

$$J_{\text{D}} = (2/3)(2/3)^{0.5} B_{\text{Crit,th}} / (\mu_0 \lambda_{\text{L}}) \quad (1)$$

with $B_{\text{Crit,th}}$ the thermodynamic critical magnetic field (its flux density), μ_0 the electromagnetic vacuum constant and λ_{L} the field penetration depth; the derivation of J_{D} is explained, e.g. in [16]. Strictly speaking, Eq. (1) is valid for type I superconductors only. If we tentatively insert the lower critical field, $B_{\text{Crit,1}}$, of a type II superconductor like BSCCO (instead of $B_{\text{Crit,th}}$, to obtain an estimate of a lower limit of J_{D}), we even then have very large J_{D} (the results shown in Fig. 14). These are much larger than the J_{Crit} that, as usual, are limited by flux flow. Yet transport current density, J_{Transp} , at temperature close to T_{Crit} might exceed J_{D} (because of its temperature dependence) and create quasi-particle (normal resistive) states.

If J_{Transp} exceeds J_{D} , electron pairs will decay, and a time τ_{R} is needed to establish new equilibrium charge distributions in the superconductor; this time has to be estimated in order not to collide with integration times, δt , of Fourier's

equation, compare [17]. This period covers total redistribution of electron pairs to ground state, at a given temperature, of the superconductor; in an FE scheme, it would request also exchange of charge between neighbouring elements. Estimates yield $\tau_R < 10^{-6}$ s [17] except for temperatures very close to critical temperature. Integration times, δt , have to be chosen safely larger than this value. A value $\tau_{Th} < \tau_R$ would be meaningless.

Accordingly, in order to determine transient resistive states of all kinds and in all constituents of the conductor, the following relations have to be checked, separately in each superconductor element of the FE scheme, and with appropriately chosen time integration steps,

$$T \leq T_{Crit}(B), \text{ with } T = T(x, y, t) \text{ and } B = B(x, y, t) \text{ and} \tag{2a}$$

$$J_{Transp} \leq J_{Crit}(T, B), \text{ with } J_{Transp} = J_{Transp}(x, y, t), \\ T = T(x, y, t) \text{ and } B = B(x, y, t) \text{ and} \tag{2b}$$

$$J_{Transp} \leq J_D(T, B). \tag{2c}$$

and the total resistance of superconductor elements be compared with the total resistance of the Ag-matrix.

In summary of Section 2, the new FE scheme allows to visibly (and more clearly than before) correlate spatial distribution of the resistances (flux flow and Ohmic vs. zero loss resistance states) and the resulting distribution of transport and over-currents.

3 Results

3.1 Comparison Between Results from Different Finite Element Schemes

A first calculation serves for comparison of total transport current shown in the previous ([7], Fig. 8) with the present paper (Fig. 3). Data obtained in [7] are indicated by solid blue diamonds and solid black triangles; those calculated in the present paper are given by corresponding open symbols. Results are shown for two different conductor lengths and two different magnitudes of normal conductor resistance (the normal conductor component in Fig. 2).

As mentioned, the results obtained in [7] were calculated using a cylindrical geometry of a quasi-continuous distribution of “threads” (a model conductor). Data obtained in the present paper are calculated using the conductor geometry shown in Fig. 1b. Comparison in Fig. 3a accordingly is

made between two different finite element models (quasi-continuum vs. multi-filamentary) but with same (model conductor) materials properties. Overall agreement shows that the previously modelled conductor was an acceptable approximation, at least for calculation of integral properties like conductor stability functions.

It is tempting to assume that current transport not only in monolithic (like thin film) but also in multi-filamentary, poly-crystalline superconductors could be analysed in terms of percolation theory. A first result supports this expectation: Fig. 3b shows current re-distribution in the conductor cross section in different planes $z = \text{const}$ in the conductor x, y -cross section; planes are identified by different colours. Results have been obtained with the continuum model applied in [7]. Data are shown at $t = 3, 6$ and 9 ms (diamonds, triangles and spheres, respectively).

Comparison at $t = 3$ and 9 ms (or between $t = 6$ and 9 ms) shows that different symbols (diamonds and circles, or triangles and circles, respectively) but of same colour do not coincide, at any radial position. This indicates transport current is continuously re-distributed, from $z = \text{const}$ planes to the next planes (including current sharing by its transfer to the matrix) *as if* current percolates through the superconductor. If this is indeed a still to be verified, appropriate approach, it might help to more specifically analyse conductor stability against quench (only some comments can be made presently, to stimulate discussion of this concept; see Section 3.4).

3.2 Temperature Fields

Temperature fields and stability functions are presented in the following using solely the new (discrete) FE geometry (Fig. 1b) and appropriate BSCCO 2223 materials and transport properties.

In-homogeneity of temperature, even in the tiny filaments, arises already before conductor temperature exceeds critical temperature (Fig. 4a–c). In-homogeneity is enhanced, and hot spots become more pronounced, at still higher temperatures (Fig. 4d).

Relative temperature maxima in Fig. 4a–d are located at large co-ordinates, y , and this must be reflected by the distribution of transport currents since critical current density, $J_{Crit}(x, y, t)$, that limits transport current density in zero loss situations, depends on temperature. Figures 5a, b and 6a, b confirm this expectation (and this conclusion can be made already by inspection of Fig. 3b).

In-homogeneity of temperature distribution results from an imbalance between generation of local losses and redistribution (thermalisation) of these losses within the

conductor and to the coolant. Thermal diffusivity parallel to c -axis, toward the solid/coolant interface, in BSSCO (2223) is about a factor 100 smaller than in x -direction (τ_{Th} then is in the order of 0.6 ms). All superconductor temperatures are above T_{crit} already at 9 ms. Even if losses would be set to zero for all $t \geq 10$ ms, recovery to below T_{crit} will not be achieved before several hundred milliseconds.

Figure 7a shows temperature difference $\Delta T(x, y = 260 \mu\text{m})$ between solid/liquid interface and (constant) coolant temperature in dependence of the x -coordinate (the axis of symmetry is located at $x = 1920 \mu\text{m}$). Because of the comparatively large Ag-“block” at small x (less density of heat sources), conductor temperature and ΔT naturally become considerably smaller than at positions close to the axis. All these results rely on applicability of the stationary heat transfer data reported in [15]. This needs more discussion.

3.3 Heat Transfer

Assume in the following that parallel to and through the conductor bundle, coolant flows in narrow channels and directly wets the conductor on its upper surface (Fig. 1b). Formation of single, isolated nitrogen vapour bubbles on a flat surface, in a variety of liquids, takes about 5 to 10 ms after onset of a disturbance like a heat pulse; the period depends on strength of the disturbance and on surface roughness (difference between flat and curves surfaces will be neglected in the following). Fully developed, stationary pool boiling is not accomplished before about 200 ms; see Fig. 7 in [21] (measurements taken with a directly wetted metallic surface; neither orientation of the vertical channel nor its width of 4 mm should be too serious a handicap when comparing with the present case). The “jump”, from initial conduction to pool and film boiling, would take at least this period of time. The same argument, at earlier periods, applies to onset of convection (no phase-change).

The following comment concerns the frequently made assumption of adiabatic conditions and modelling of stationary heat transfer. If there is a periodic heat source in the interior of the conductor, we can imagine three situations:

(i) If its position is far from conductor surface, and if the frequency is large enough, thermal waves emitted from the source will strongly be damped, and there will be hardly any oscillation of surface temperature. Stationary heat transfer and approximately adiabatic conditions thus are justified although conductor temperature will steadily increase under heat flow continuously emitted by the source (this increase, at least as in the present situation, is small).

The situation is different if (ii) position of the oscillating source is close to conductor surface, which is the case when current is directed to the outer Ag-matrix elements (current sharing between filaments and matrix). This is demonstrated in Fig. 7a. With increasing load (at increasing time), surface (nodal) temperature becomes variable with position (x -coordinate). These variations, at constant time, reflect position of filaments in the interior of the conductor (the centrally located hot spots in the filaments) but location of the maxima of ΔT also depends on time (this is not to be confused with a phase difference). Obviously, assumption of stationary heat transfer would be erroneous since local variation of surface temperature is too strong, for example, about 6 K at $t = 8.71$ ms. Curves ΔT like in Fig. 7a of course could be fabricated also for larger times, but this collides with the observation that already at $t \leq 8$ ms, thermal losses increase very strongly, due to the strong non-linearity of all parameters and processes involved, so that application of the stationary heat transfer data from [15] would become very questionable.

One could argue that application of an insulating layer that covers the conductor surface would justify application of stationary heat transfer data as well as the adiabatic approximation. Such an insulating layer is generated by the liquid when it enters the film boiling regime. But this will happen only if there is a large temperature difference between surface and coolant, in contradiction to the adiabatic assumption.

Heat fluxes are shown in Fig. 7b. The values, at these positions and at these times, are below 0.1 W/cm^2 , heat transfer accordingly is still in the convection regime and comparison with the data reported in [21] is meaningful. The situation changes drastically when $t > 9$ ms is considered; heat fluxes then become in the order of 100 W/cm^2 . This is the situation (iii): under very large load, onset of boiling heat transfer is realised the earlier the higher the load (compare Fig. 7c for explanation). The adiabatic assumption then is no longer valid, and it is also highly questionable whether this situation still could correctly be handled with the stationary heat transfer data from [15].

An alternative is to reduce the load but then surface temperature hardly increases (compare the lower curves in Fig. 7a); the strong non-linearity of the transport problem is obvious.

Investigation of extreme load cases thus should be performed only when reliable, transient heat transfer data will become available; this would also be helpful to avoid convergence problems. Calculations under very large load presently cannot be successful.

In the present paper, with the Ag/coolant interface (and not with non-conductor surfaces), and as long as load is small (to yield heat flux at the solid/liquid interface of below 0.6 W/cm², compare [21] for this limit), a mismatch is obvious between *calculated* (by the FE scheme) time to arrive at convection, pool and film boiling, and time *physically* needed to trigger initial movement of the liquid and to create bubbles and films (these are the data reported in [21]; the concept is illustrated in Fig. 7c). Calculated time is much smaller than physically needed time. This mismatch can allow application of the heat transfer data from [15], with thermal load below 0.6 W/cm² on the solid/liquid interface.

In summary of this subsection, there are in general no uniform heat transfer conditions in transient experiments over the entire interface, neither in time (stationary conditions) nor with respect to surface position (adiabatic assumption).

3.4 Stability functions

Stability functions provide an integral view of critical current density distribution in a conductor and thus of its ability to transport current without losses. Calculations of the stability functions have been performed following the explanations given in [7], Section 4. We emphasise that again, the calculations have to be made with critical current densities depending not only on local temperature but also on local magnet flux density because $J_{\text{Transp}} > J_{\text{Crit}}$, too, constitutes a disturbance (by generation of flux flow losses; these alter local temperature and thus local J_{Crit}).

We apply as an approximation the standard relation

$$J_{\text{Crit}}(T, B) = J_{\text{Crit}}(T)/(B_0 + B(t)) \tag{3}$$

with local flux density, $B(t)$, and B_0 a constant. The stability function reads

$$0 \leq \Phi(t) = 1 - \int J_{\text{Crit}}[T(x, y, t), B(x, y, t)]dA / \int J_{\text{Crit}}[T(x, y, t_0), B(x, y, t_0)]dA \leq 1 \tag{4a}$$

This is approximated by

$$0 \leq \Phi(t) = 1 - \Sigma J_{\text{Crit}}[T(x, y, t), B(x, y, t)]dA / \Sigma J_{\text{Crit}}[T(x, y, t_0), B(x, y, t_0)]dA \leq 1 \tag{4b}$$

with the summations taken over all superconductor elements with their individual cross sections, dA .

The stability function assumes values $0 \leq \Phi(t) \leq 1$, of which $\Phi(t) = 0$ are the optimum and $\Phi(t) = 1$ the worst case: time $t_0 = 0$ denotes start of the present simulation; at this time, all element temperatures are at their original values, $T(x, y, t_0) = 77$ K, at a given $B(x, y, t_0)$. Critical current density, $J_{\text{Crit}}(x, y, t_0)$, then is maximum, and $\Phi(t_0) = 0$. The distribution of J_{Crit} at t_0 accordingly is homogeneous, apart from statistical fluctuations caused by the random $J_{\text{Crit}0}$ (the materials property, compare [7], Fig. 12). But homogeneity is quickly lost at times $t > t_0$.

If on the other hand, $\Phi(t) = 1$, *zero loss* current transport is no longer possible, see below, Eq. (5).

Results for the stability function using BSCCO materials properties are shown in Fig. 8. There are almost no differences between the results obtained with the larger or smaller number of elements, N_{El} . For comparison, also results are included that are obtained with the materials properties of YBaCuO (123), under the same conductor geometry and FE scheme (it is clear, from manufacture issues, that the YBaCuO material is not very well suited for fabrication of 1G conductors). In both cases, the stability functions at times $t > 8$ ms approach values close to 1. Maximum zero loss transport current, $I_{\text{max}}(t)$, with A_{SC} the total conductor cross section,

$$I_{\text{max}}(t) = J_{\text{Crit}}[T(x, y, t_0), B(x, y, t_0)][1 - \Phi(t)]A_{\text{SC}} \tag{5}$$

thus becomes close to zero since many of the $T(x, y, t)$ within the filaments are close to or exceed $T_{\text{Crit}}(x, y, t)$, compare the hot spots in Fig. 4a–d that in turn drive conductor temperature to inhomogeneous distributions. The onset of the sharp increase of $\Phi(t)$ reflects the lower T_{Crit} of the YBaCuO superconductor material but predicts the in-homogeneity problem also for this conductor.

In Fig. 4a–f, only tiny parts of their individual cross sections have become normal conducting (hot spots generated at these positions). Current limitation, if any, in the conductor in Fig. 1b, at least until $t \leq 9$ ms, accordingly would rely on Ohmic resistance in only these small parts of the filament cross sections while in the remaining parts zero resistance or flux flow resistance would co-exist, side by side, with the said Ohmic resistances. At later times, $t \leq 12.5$ ms, all element temperatures exceed the individual $T_{\text{Crit}}(x, y, t)$ but in-homogeneity remains; note that these results include already transfer of over-current to the matrix (current

sharing). Transfer of over-current, for example, to a shunt, may compensate this critical situation but the superconductor materials properties might already be damaged locally before this can be realised. A mechanism (purely flux flow or Ohmic resistance) that would trigger switching the over-current to the shunt or to an equivalent experimental device cannot uniquely be identified. The same applies to a situation when no shunt would be incorporated into the circuit.

Spatial distribution of the specific resistances (zero, flux flow and Ohmic) is illustrated in Fig. 9 (location of Ohmic resistances, not shown in this figure, can easily be identified from Fig. 4a–f). Flux flow resistances exist in parallel to Ohmic resistances. At least within these periods of time, there is no clear distinction between Ohmic or flux flow fault current limiting.

3.5 Correlation with Percolation Theory

Like a liquid through a sponge, current may percolate through a monolithic or porous or multi-filamentary conductor. Current paths are opened, under variation of materials properties or of operation conditions, as soon as a percolation threshold is approached.

Transition to superconductivity could be correlated with a percolation threshold that is based on regions of, for example, different critical temperature, compare [22]. But it is not clear that any percolation concept would be applicable to also multi-filamentary conductors.

There will always be current flow, under zero or under flux flow or Ohmic resistive conditions, through the conductor cross section and also under current sharing with the matrix. A threshold thus may reasonably be defined only with respect to zero losses. This would be observed when at least one path (channel) is open to current flow over the whole conductor length, *and* if it incorporates only elements in the Meissner state. Under current sharing with matrix elements, or if the over-current is fed to a shunt, there is no zero loss current transport at all. In an attempt to describe current transport as a percolation process, the analysis has to be restricted to only the superconductor filaments in the cross section; otherwise, definition of the threshold becomes meaningless.

Under this restriction, the question is whether a correlation might exist between stability functions and percolation threshold: non-zero loss current transport is possible only if the stability function $\Phi(t) < 1$. Percolation thresholds then may be observed if $\Phi(t)$ is checked with different (mean) values of critical current density, critical temperature or magnetic fields. A threshold is identified when suddenly, under such parameter variations, $\Phi(t)$ breaks down to values close to zero. But $\Phi(t) < 1$ does not indicate there will

be one and only *one* zero loss transport channel: Extended domains composed of zero loss, coherent channels can exist in the cross section, and this may be different in different planes $z = \text{const}$. Also, $\Phi(t) < 1$ does not guarantee there will necessarily be *any* nonzero number of open, straight-ahead channels coherently connected over total conductor length. Note that Eq. (4a,b) contains only local *values* of J_{Crit} ; no restriction is incorporated in this equation that the elements might be inter-connected; elements with large J_{Crit} can be distributed almost arbitrarily in the whole conductor volume without generation of such open channels. Apparently, there is no clear correlation between stability functions and standard percolation models.

This question will be investigated in more detail in a subsequent paper; the analysis needs inclusion of a z -dependence of material parameters, a challenging task in view of the present numerical problems.

4 Conclusion

Under a transient load, analysis of current transport in a multi-filamentary superconductor requires simulations with high spatial and time resolution. Time integration has to take into account at least three characteristic times that concern electric/magnetic current and field propagation, thermal transport and depairing (decay) and electron pair re-combination and re-population processes of the energy levels (times τ_{El} , τ_{Th} , τ_{R} , respectively). Ohmic, flux flow and zero resistance states may co-exist in the conductor if transport and fault over-currents cannot be compensated (for example, shifted to a shunt). With or without shunt or equivalent experimental measures, a clear distinction, taken over the total conductor volume, between purely Ohmic resistance or flux flow resistance is not possible for periods immediately following onset of a disturbance. Traditional differentiation between, for example, flux flow or Ohmic resistance type fault current limiters becomes highly questionable. Stability functions apparently are not correlated with standard current percolation theory. An appropriate percolation model could be helpful for stability analysis in multi-filamentary conductors; this needs more discussion. In transient experiments, there are in general no uniform heat transfer conditions over the entire interface, neither in time nor with respect to surface position; application of stationary heat transfer data and assuming adiabatic conditions may be acceptable only under very limited thermal load. The achieved results may become important to improve understanding of current transport in general and in a variety of technical applications of superconductivity (cables, magnets, current limiters).

Appendix

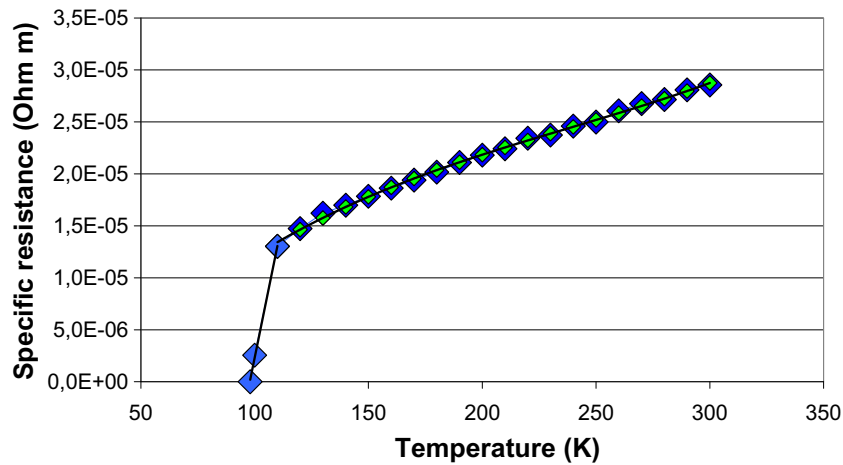


Fig. 10 Specific electrical Ohmic resistance to current transport in z -direction of solid BSCCO 2223 material (*solid blue diamonds*). Data are from [18]. *Solid light green diamonds* indicate approximation to the experimental data

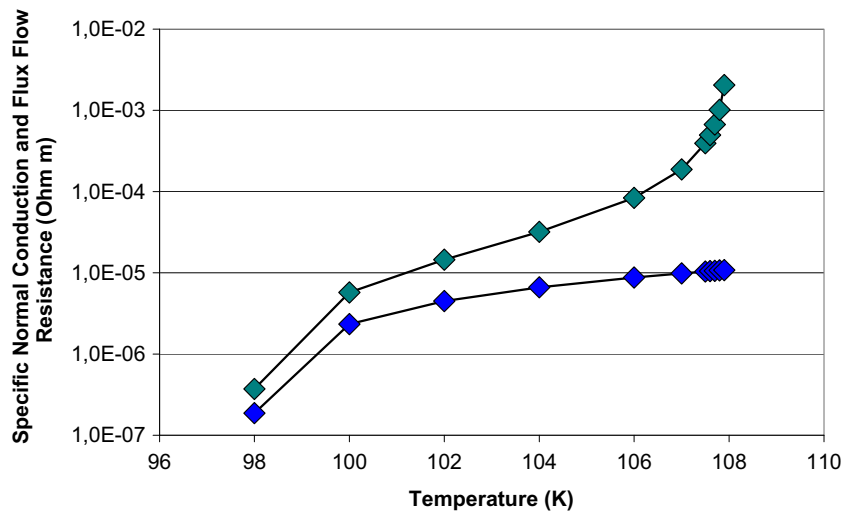


Fig. 11 Specific flux flow resistance (*solid green diamonds*) to current transport in z -direction under moving flux quanta in x -direction (Fig. 1b) in porous BSCCO 2223 material (grains, with weak links in-between). Because of the temperature dependence of the upper critical magnetic field, the curve diverges near T_{crit} . The *solid blue diamonds*

indicate specific electrical resistance without inclusion of flux flow (same data as in Fig. 10), both curves within $98 \leq T \leq T_{\text{crit}}$ ($B = 0$), of solid BSCCO material. The large difference between the two curves results from the estimated contribution of grain boundaries (weak links). Results are obtained with $B = 100$ mT.

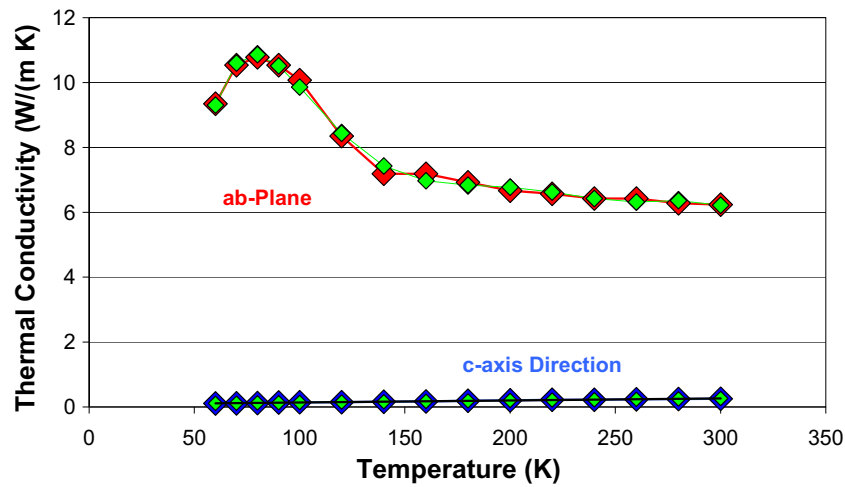


Fig. 12 Thermal conductivity of BSCCO 2223 (solid red and blue diamonds). Data are from [19]. In both curves, solid light green diamonds indicate approximations to the experimental data

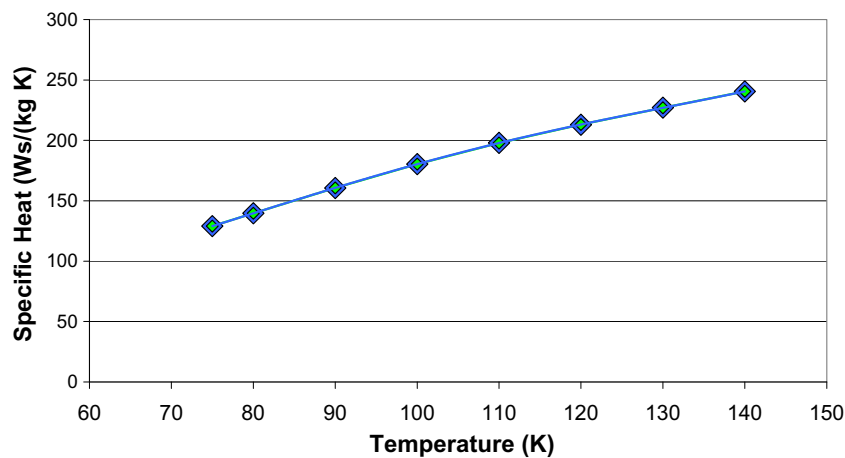


Fig. 13 Specific heat of BSCCO 2223 (solid blue diamonds). Data are from [20]. Solid light green diamonds indicate approximations to the data

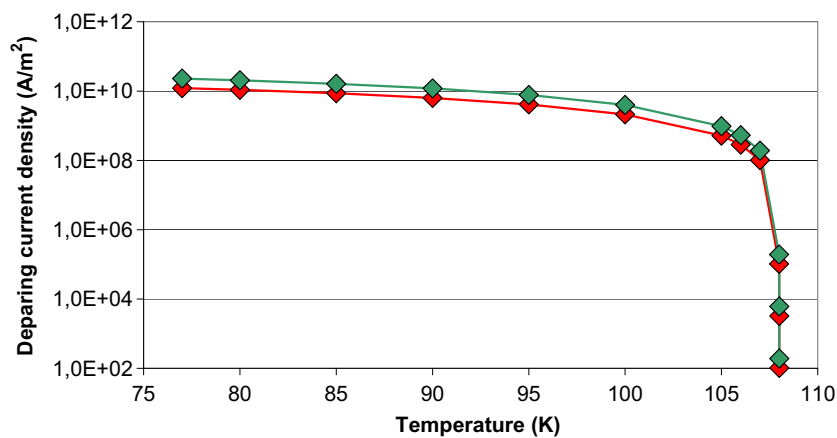


Fig. 14 Depairing current density, J_D , of BSCCO (2223) in a - and b -directions (solid red and green diamonds, respectively) of the ab -plane. For this calculation, Eq. (1) is tentatively applied to BSCCO though it is strictly valid only close to T_{crit} and for type I superconductors. The figure shows lower values of J_D because $B_{\text{crit},1}$ instead of $B_{\text{crit},\text{th}}$ has

been used in Eq. (1). Values of the mean penetration depth, λ_a and λ_b , of a - and b -directions have been applied for this calculation. For the λ values, see [16], Tab.2. 7 (in Fig. 4.8 of the same reference, values of λ_a and λ_b are mentioned for YBaCuO, and may be taken for comparison)

References

- Blatt, J.M.: Theory of Superconductivity. Academic Press, New York and London (1964)
- de Gennes, P.G.: Superconductivity of Metals and Alloys. W. A. Benjamin, Inc., New York and Amsterdam (1966)
- Tinkham, M.: Introduction to Superconductivity. Robert E. Krieger Publ. Co., Malabar (1980). repr. Ed.
- Wilson, M.N.: Superconducting Magnets. In: Scurlock, R. (ed.) Monographs on Cryogenics. Oxford University Press, New York, reprinted paperback (1989)
- Dresner, L.: Stability of Superconductors. In: Wolf, St. (ed.) Selected Topics in Superconductivity. Plenum Press, New York (1995)
- Kalsi, Sw.S.: Applications of High Temperature Superconductors to Electric Power Equipment, pp. 173–217, Hoboken (2011)
- Reiss, H.: Superconductor stability against quench and its correlation with current propagation and limiting. *J. Superconduct. Novel Magn.* **28**, 2979–2999 (2015)
- Rettelbach, T., Schmitz, G.J.: 3D simulation of temperature, electric field and current density evolution in superconducting components. *Supercond. Sci. Technol.* **16**, 645–653 (2003)
- Marzahn, E.: Supraleitende Kabelsysteme, Lecture (in German) given at the 2nd Braunschweiger Supraleiter Seminar, Technical University of Braunschweig (Germany) <https://www.tu-braunschweig.de/Medien-DB/iot/s-k.pdf> (2007)
- Shimizu, H., Yokomizu, Y., Goto, M., Matsumura, T., Murayama, N.: A study on required volume of superconducting element for flux flow resistance type fault current limiter. *IEEE Transacts. Appl. Supercond.* **13**, 2052–2055 (2003)
- Diaz, A., Mechin, L., Berghuis, P., Evetts, J.E.: Observation of viscous flow in $\text{YBa}_2\text{Cu}_3\text{O}_7$ – low-angle grain boundaries. *Phys. Rev. B* **58**(6), R2960–R2963 (1998)
- Hao, Zh., Clem, J.R.: Viscous flow motion in anisotropic type-II superconductors in low fields. *IEEE Transacts. Magn.* **27**, 1086–1088 (1991)
- Reiss, H.: Radiation heat transfer and its impact on stability against quench of a superconductor. *J. Superconduct. Nov. Magn.* **25**, 339–350 (2012)
- Reiss, H., Troitsky, O.Yu.: Superconductor stability revisited: Impacts from coupled conductive and thermal radiative transfer in the solid. *J. Superconduct. Novel Magn.* **27**, 717–734 (2014)
- Fastowski, W.G., Petrowski, J.W., Rowinski, A.E.: Kryotechnik (In German). Akademie-Verlag, Berlin (1970)
- Buckel, W., Kleiner, R.: Superconductivity, Fundamentals and Applications, Transl. by Huebener, R., 2nd edn. Wiley (2004)
- Reiss, H.: A microscopic model of superconductor stability. *J. Superconduct. Novel Magn* **26**(3), 593–617 (2013)
- Khan, M.N., Zakaullah, K.h.: Novel techniques for characterization and kinetics studies of Bi-2223 conductors. *J. Res. (Sci.)* **17**(1), 59–72 (2006)
- Fricke, J., Frank, R., Altmann, H.: Wärmetransport in anisotropen supraleitenden Dünnschichtsystemen, Report E 21 - 0394 - (1994). In: Knaak, W., Klemt, E., Sommer, M., Abeln, A., Reiss, H. (eds.) Entwicklung von wechselstromtauglichen Supraleitern mit hohen Übergangstemperaturen für die Energietechnik, Bundesministerium für Forschung und Technologie, Forschungsvorhaben 13 N 5610 A, Abschlußbericht Asea Brown Boveri AG, Forschungszentrum Heidelberg (1994)
- Schnelle, W.: Spezifische Wärme von Hoch- T_c Supraleitern, Doctoral Thesis, University of Cologne, Germany (1992)
- Drach, V., Hemberger, F., Ebert, H.-P., Körner, W.: Heat transfer into vertically oriented channels filled with liquid nitrogen, ZAE Bayern, Wuerzburg, Germany, Report ZAE 2 - 0898 - 1 (1998)
- de Mello, E.V.L., Caixeiro, E.S., González, J.L.: A novel percolation theory for high temperature superconductors. *Braz. J. Phys.* **32**, 705–709 (2002)